Two-Dimensional Surface Dopant Profiling in Silicon Using Scanning Kelvin Probe Microscopy

Albert K. Henning, Todd Hochwitz

Thayer School of Engineering Dartmouth College Hanover, NH 03755

James Slinkman, James Never, Steven Hoffmann, Phil Kaszuba

IBM Microelectronics Essex Junction, VT 05452

Charles Daghlian

Rippel Microscopy Facility Dartmouth College Hanover, NH 03755

November 3, 1994

Abstract

We have applied a simultaneous combination of scanning Kelvin probe microscopy and scanning atomic force microscopy to the problem of profiling dopant concentrations in two dimensions in silicon microstructures. By measuring the electrochemical potential difference which minimizes the electrostatic force between probe tip and sample surface, we estimate the work function difference between the tip and surface. To the extent that this work function difference is a consequence of the dopant concentration at, or near, the sample surface, we infer doping profiles from our measurement. Structures examined and presented here include contact holes, and the technologically significant lightly-doped drain of a metal-oxide-silicon field-effect transistor. Using this methodology, we are able to distinguish relative changes in dopant concentration with lateral resolution less than 100 nm. Sample preparation is minimal, and measurement time is fast compared to other techniques. Our measurements have been compared to predictions based on two- and three-dimensional process and device simulation tools. The comparisons show our technique is sensitive to changes in dopant concentration, from $\approx 10^{15}$ cm^{-3} to 10^{20} cm^{-3}, of less than ten percent at these size scales. Suggestions to resolve absolute dopant concentration are made.

1 Introduction

Measurement of doping profiles in silicon and gallium arsenide (GaAs) devices on micron and sub-micron scales has long been a goal for process and device engineers. One-dimensional profile measurement has been available since the middle 1970s. However, in silicon bipolar, silicon metal-oxide-semiconductor field-effect transistors (MOSFETs), and GaAs-related heterostructure devices, accurate knowledge of two- and even three-dimensional profiles is required in order to predict device performance and reliability. Corroboration of process simulator predictions of heterostructure and doping profiles, with the actual profiles themselves, therefore becomes increasingly important as sub-micron dimensions are achieved in manufacturing practice.

The central goal of our work is to develop Scanning Kelvin Probe Microscope (SKPM) as a leading means to measure two-dimensional (2D) dopant concentration profiles. Spatial resolution near 25 nm, and absolute dopant concentration accuracy of ten percent, over the full range of dopant densities important to semiconductor device design and fabrication, will be necessary in order to achieve this goal.

Extensive reviews of most available profiling techniques, in one, two, and three dimensions, have been presented [1,2], and will not be repeated here. Techniques specific to 2D

dopant profiling in silicon are important to our work, however, and are worth summarizing briefly.

Scanning Capacitance Microscopy (SCM) [3,4] is the leading 2D dopant profiling technique at this time. Sample preparation is minimal. Plan-view measurements are non-destructive, while cross-sectional measurements require scribing and breaking the sample. Measurements are taken in air. Lateral resolution is limited to twice the probe tip radius, roughly 100 nm at present. Dopant concentrations may be imaged in the 10^{16} cm^{-3} – 10^{21} cm^{-3} range. Accuracy is sufficient to allow comparison with numerical process simulation tools, though as yet insufficient to allow distinction between subtle changes in dopant diffusion models. A single sample suffices to obtain an entire profile. Computer data deconvolution is required. Improvements in accuracy will require calibration against well-defined experimental matrices, yielding samples with doping profiles well-characterized by more traditional means.

Secondary-ion mass spectrometry (SIMS) has been used in conjunction with samples beveled on multiple angles [5,6], or etched in vertical relief at an angle to an implanted edge [7]. Analysis proceeds using computer tomographic techniques. The technique is destructive, time-consuming, and requires multiple samples to achieve a single profile, but is otherwise successful in meeting many of the 2D dopant profiling goals.

Spreading resistance combined with mechanical magnification using angled and beveled etching has recently achieved $10^{12} - 10^{19}$ cm^{-3} sensitivity with 25-50 nm lateral spatial resolution [8]. Computer deconvolution of the data is required.

An optical technique has been successful in detailing profiles in the $10^{14} - 10^{19}$ cm^{-3} range, with lateral resolution of 40 nm [9]. Relatively time-consuming sample etching and beveling is required. Multiple samples are required, one for each isoconcentration line in the profile.

Atomic Force Microscopy combined with controlled etching has been used with some success to decorate dopant profiles [10]. Control of the etch solutions, and calibration of etch rates against sample with well-known dopant concentrations, have yet to be established.

2D profiles have been inferred using a coupling between simulation, and electrical measurement of source-drain overlap capacitance in a MOSFET [11,12]. The interplay between simulation and measurement can be tedious, and subject to the specifics of the simulation transport and capacitance models. Additional test structures to obtain, for instance, gate-to-drain overlap capacitances, must be fabricated and measured. The technique is non-destructive, and requires a single sample to obtain profile data, but is specific to the MOSFET structure, making generalization to other structures problematic.

Previous experimental results have shown that simultaneous use of a Scanning Atomic Force Microscope (AFM) and SKPM can provide qualitative dopant concentration profiles [13–17]. In this work we attempt to lay the foundation for determining a quantitative relationship between measurements obtained through the use of SKPM and the theoretical 2D dopant profiles in silicon microsctructures. Compared to the previous methods outlined above, we believe this technique offers the best means to achieve our goals. To date, our lateral XY positional precision is regularly 50 nm; we have achieved 15-25 nm with some care. Our vertical Z positional resolution is $\approx$ 1 nm in AFM mode. In SKPM mode, we have achieved a measurement sensitivity of 1 mV/$\sqrt{\text{Hz}}$, which translates at our measurement frequencies to a resolution of roughly 5 mV. We believe a resolution of 0.5 mV is achievable. Such resolution in the measured electrochemical potential difference (EPD) between tip and surface yields easily the sensitivity to distinguish dopant concentration changes over the 10^{15} cm$^{-3} - 10^{20}$ cm^{-3} range. Due to probe tip geometry, signal convolution between tip and surface, and masking effects at the surface, we are only able to infer changes in dopant concentration with a lateral resolution of 50 nm to 100 nm. Our present technique will require calibration to known dopant concentration standards, or advances in understanding and control of the probe tip/sample surface system, in order to achieve our desired absolute accuracy.

2 Description of Measurement Technique

2.1 System Description

Our SKPM is a non-contact AFM built at IBM – Yorktown Heights, to which we have added the necessary hardware for implementing the Kelvin measurement technique [18].

Figure 1 shows a block diagram of the major components for the SKPM. The deflection of a force sensing cantilever is detected with a heterodyne-based interferometer [19]. The heterodyne system allows us to monitor the deflection of the cantilever simultaneously at several different frequencies. One frequency is used for the force gradient loop, another for the Kelvin loop [20]. The harmonic of the Kelvin excitation frequency is used to obtain the $\frac{\partial C}{\partial z}$ signal. We are able to locate several peaks in the frequency response of the cantilever's deflection for operational use since it behaves as a lumped mass system.

A Wye Creek Piezoflex stage with a PFC-2-AA controller [21] is used to perform XY translation of the cantilever during a scan. The Z translation and force gradient excitation are performed with a single bimorph. The sample remains stationary during a scan.

A Hewlett-Packard 3325B frequency generator is used to excite the bimorph. This provides the signal necessary for tracking the force gradient contours. The force gradient

lock-in amplifier and feedback servo are custom designs built at IBM – Yorktown Heights. The output of the force gradient servo is used to perform Z translation of the bimorph by the proper amount to keep the probe tip-sample spacing such that the measured force gradient remains constant. The output of the force gradient servo is used as an estimate of the surface topography. The data is acquired with an IBM PC/AT via one channel of a Data Translation DT2827 analog-to-digital conversion board [22].

A Princeton Applied Research (PAR) model 124A lock-in amplifier [23] with a model 116 differential pre-amp is used to generate the *ac* component of the Kelvin signal and to detect the corresponding deflection of the cantilever due to the electrostatic force. The Kelvin feedback servo was designed and built at Dartmouth College. It uses the signal from the output of the Kelvin lock-in to adjust the DC component of the potential between the probe tip and the sample to minimize the electrostatic force. The output of the Kelvin servo is acquired at the same time as the force gradient contour data via a second channel of the DT2827.

A PAR model 5301 lock-in amplifier with a model 5315 two channel pre-amp is used to monitor the deflection of the cantilever at twice the Kelvin frequency in order to obtain the $\frac{\partial C}{\partial z}$ information. At this time no attempt is made to servo the *ac* component of the potential between the tip and sample to maintain a constant value for the $\frac{\partial C}{\partial z}$ signal. We

currently use the $\frac{\partial C}{\partial z}$ information only for qualitative analysis. It is acquired at the same time as the force gradient and surface potential contour data via a third channel of the DT2827.

2.2 System Operation

Our SKPM has been used successfully with electrochemically etched tungsten probe tips and micro-fabricated silicon probe tips from IBM [24]. Some of the silicon probe tips used were coated with 10 to 20 nm of gold to increase tip conductivity [24]. We have obtained comparable results when using gold coated and uncoated silicon tips. This may be an indication that the gold coating flakes off of the tips during the scans, requiring ultimately a better material for coating.

We have run the SKPM in two different configurations. In one configuration (see Figure 1) the sample is grounded and the Kelvin servo and excitation signals are applied to the tip. This configuration requires electrical isolation between the z translation bimorph and the probe tip, which is accomplished with a glass cover-slip. The second configuration grounds the tip to one side of the bimorph, and the Kelvin servo and excitation signals are applied to the sample. Experiments have shown that both configurations yield equivalent scans for the samples we have examined.

The z translation bimorph is excited at a frequency slightly higher than the strongest

resonant frequency of the cantilever. For the tungsten tips this frequency is between 90 kHz and 150 kHz, and for the silicon tips it is between 300 kHz and 500 kHz. Shifts in the resonant frequency of the cantilever cause a change in the amplitude of the cantilever at this excitation frequency. The resonant frequency shifts arise from changes in the force gradient due to spatial topography variations. The DC component of the bimorph input is adjusted to bring the cantilever amplitude back to the desired magnitude. The voltage applied to the bimorph is measured, and may be used as an estimate of the surface topography after we have calibrated the system (discussed in the following section).

The electrochemical potential:

$$U(t) = U_{DC} + V_{ac}\sin(\omega t) \tag{1}$$

between the tip and sample is modulated at a frequency ω corresponding to one of the other strong vibrational modes of the cantilever. The PAR lock-in amplifiers we currently use limit the Kelvin loop to frequencies under 200 kHz if we are only interested in the electrostatic surface potential, and to frequencies under 100 kHz if we are interested in both the surface potential and $\frac{\partial C}{\partial z}$ information.

It has been shown by several researchers that, in the absence of any surface or dielectric charge, the electrostatic force between the tip and surface may be approximated as [13,25,

26]:

$$F_{electrostatic} = \frac{1}{2}\Big(V_{DC} + V_{ac}\sin(\omega t)\Big)^2 \frac{\partial C}{\partial z} \tag{2}$$

where V_{DC} and V_{ac} are the DC and ac components of the electrostatic potential between the tip and the sample, C is the effective capacitance between the tip and the sample, z is the distance between the tip and the sample, and ω is the frequency at which the potential is being modulated. Expanding the potential terms results in the following relationship between the electrostatic force and the potential:

$$\begin{aligned} F_{electrostatic} &= \frac{1}{2}\left(V_{DC}^2 + \frac{1}{2}V_{ac}^2\right)\frac{\partial C}{\partial z} && (3)\\ &+ \frac{\partial C}{\partial z} V_{DC} V_{ac}\sin(\omega t) && (4)\\ &- \frac{1}{4}\frac{\partial C}{\partial z} V_{ac}^2\cos(2\omega t) && (5) \end{aligned}$$

With the heterodyne interferometer we are able to monitor the deflection of the cantilever at ω and 2ω, yielding signals proportional to Equations 4 and 5. The DC component of the electrochemical potential U_{DC} between the tip and the sample is adjusted to minimize the signal detected at a frequency of ω. Adjusted so, U_{DC} becomes an estimate of the work function difference (WFD) between the tip and the sample (see Figure 2). This interpretation of U_{DC} is central to an understanding of the SKPM dopant profiling technique. The accuracy of the estimate will depend upon: the magnitude of stray capacitance sig-

nals associated with the cantilever; the screening effect of surface charges; and the spatial inhomogeneity of both structural shape and dopant profile.

The signal detected at 2ω is rectified and filtered to obtain an estimate for the spatial variations in $\frac{\partial C}{\partial z}$. It provides an additional means to image structural and material characteristics of the sample surface.

A force based Kelvin probe has some advantages over the traditional vibrating capacitor technique for measuring work function differences [27–29]. For instance, taking the electrical measurements simultaneously with the force gradient measurements keeps the tip-to-sample spacing constant. This reduces the impact of spacing dependent errors which can affect other Kelvin systems [30–32].

Another advantage is the sensitivity of the force based Kelvin probe to small changes in the electrostatic force. A stable heterodyne interferometer has been shown to have a spectral sensitivity to cantilever deflections of 10^{-4} $\mathring{\text{A}}/\sqrt{\text{Hz}}$ [19], which corresponds to a WFD sensitivity of about 50 $\mu\text{V}/\sqrt{\text{Hz}}$ for silicon based tips operating in air [20]. This sensitivity is below the range of values published for the vibrating capacitor based Kelvin probes. It has also been shown that the AFM is sensitive enough to detect single units of charge [33].

A third advantage is the ability to measure the $\frac{\partial C}{\partial z}$ signal at the same time as the tip-

to-surface EPD (Kelvin signal) when scanning semiconductors. This signal has provided us with qualitative information related to surface defects, undetected by either the force gradient or Kelvin signals [34]. It may also play a role in analyzing the nature of dopants below the surface when the Kelvin loop is locked to a fixed, non-zero electrostatic force, instead of nulling out the electric field between the tip and sample [14, 34].

The use of an optical interferometer to measure the work function between the tip and sample has the advantage that parasitic capacitance in the electrical connections between the tip and input of an amplifier no longer play a role. Instead, one only needs to consider the capacitance between the tip/cantilever and the sample that give rise to the electrostatic force [35].

The most important advantage is related to lateral resolution. It is well known that the sensitivity of the vibrating capacitor based Kelvin probe decreases as the size of the tip decreases due to a reduction in the displacement current [29, 36]. With the force based Kelvin probe the limiting factors become thermal vibration of the cantilever, which is independent of the actual tip area, and the relative contribution of the cantilever to the total capacitance between the sample surface and the tip-plus-cantilever system. Therefore the force based Kelvin probe can resolve features well into the sub-micron scale. This detail is important for obtaining meaningful results on surfaces with significant amounts of

vertical relief, since the tip must be able to reach the deeper areas of any surface features.

2.3 System Calibration

Calibration of the measured force gradient for the AFM portion of our system is performed by scanning surfaces of etched SiO_2. Different thicknesses of oxide were thermally grown on the surface of silicon in the Thayer School Solid State Microstructures Lab at Dartmouth College. A simple grating pattern was then etched through the oxide to the silicon substrate. A Gaertner L104 SA two-wavelength ellipsometer [37] was used to measure the oxide thickness at various points on the substrate. Three different thicknesses are used to perform the calibration: 26 nm, 51 nm, and 550 nm. Each time the tip or bimorph is replaced, this calibration must be repeated.

The worst case sensitivity we have obtained with the force gradient loop is on the order of 1.41 $mV/\sqrt{Hz}$, which corresponds to a cantilever displacement of $\approx$ 0.212 $Å/\sqrt{Hz}$. We operate the force gradient loop at a bandwidth of 100 Hz, so the worst case vertical sensitivity is $\approx$ 0.2 nm. The best lateral resolution we have achieved has been 25 nm. The typical lateral resolution is about 50 nm. We believe the largest source of noise for the force gradient loop in our system is thermal vibration of the cantilever.

We do not currently have a corresponding "calibration standard" for the Kelvin loop. The behavior has been determined by examining the tracking ability of the Kelvin loop to

a modulated signal. A metal sample was connected to a square wave generator instead of being grounded. A 0.47 Hz square wave of variable magnitude was applied to the metal sample, and the signal from the Kelvin servo loop was monitored to see how well it followed this square wave. Peak signal magnitudes of 0.1, 0.5, and 1.0 Volts were used to determine tracking capability.

Linear fits to the potential from the Kelvin servo showed the measured voltage swing was within 5% of the applied voltage swing. For a majority of the typical feedback settings the measured signal from the Kelvin servo was within 2% of the applied signal, consistent with the specified tolerances for the electrical components used in the Kelvin servo.

The sensitivity of the SKPM for these controlled experiments was very dependent upon the feedback settings and the type of tip used. The worst values obtained were $\approx$ 40 mV/$\sqrt{\text{Hz}}$. The cleanest signals from a silicon tip yielded values of $\approx$ 5 mV/$\sqrt{\text{Hz}}$, and from a gold coated silicon or tungsten tip $\approx$ 1 mV/$\sqrt{\text{Hz}}$. We operate the Kelvin feedback loop at a variable bandwidth in the 15 Hz to 300 Hz range, depending upon the type of sample under investigation.

3 Experiments

The fabrication sequence for the first set of structures presented in this work is given in Table I. In essence, we fabricated 2.5 μm by 2.5 μm contact holes in SiO_2, and implanted

boron into these holes, on n-type (phosphorus) substrates. These samples were fabricated at IBM–Essex Junction.

After the final oxide etch, the samples were mounted on our microscope stage, and measured using the combination AFM/SKPM system we have built. Each scan required approximately thirty minutes. Note that the final oxide etch does not remove all the grown oxide, thus preserving the high-quality, low surface charge nature of the Si-SiO_2 interface.

We have also performed SKPM and AFM measurements on a MOSFET. The particular device measured was fabricated using a lightly-doped drain (LDD) technology similar to [38]. To our knowledge, no technique has yet been successful in imaging the LDD doping profile of a MOSFET. We attempted to measure such a structure, though from the surface and not in cross-section, in order to validate our technique using a problem of high technological interest.

4 Results

Figure 3 shows a one-dimensional SIMS measurement of the vertical Z doping profile. The measurement was taken in a large implanted area, given the nature of the SIMS technique. It was used to corroborate the vertical doping profile found via SUPREM-IV [39] simulation.

Figure 4 shows the SKPM measurements of 2D U_{DC} contours, which is obtained simul-

taneously with the AFM measurement (not shown).

Greyscale images of the AFM and SKPM signals obtained from the LDD MOSFET structure are shown in Figures 5 and 6.

We note that these measurements, of the XY dependence of force gradient and EPD (U_{DC}), are repeatable. Offsetting the scan window by, for instance, half a frame, shows the common portion of the two successive images to be the same.

5 Discussion

In SKPM mode, an ability to resolve 1 mV changes in U_{DC} should translate to an estimated sensitivity to changes in actual dopant concentration of +/- 5% in the vicinity of 10^{14} cm^{-3}, and +/- 8% in the vicinity of 10^{18} cm^{-3}. This estimate is determined as follows. If the tip is taken to be undoped silicon, then the EPD applied to the tip, relative to the electrically-grounded, doped substrate, necessary to null the electrostatic field is:

$$U_{DC} = (E_C - E_F)_{tip} - (E_C - E_F)_{substrate} \tag{6}$$

For acceptor doping only, and assuming the electron density has negligible impact on the determination of the Fermi level, Equation (6) becomes:

$$U_{DC} = \frac{E_g}{2} + \frac{kT}{2}\ln(N_C/N_V) - kT\ln\left[\frac{-1+\sqrt{1+16\,(N_A/N_V)\exp[E_a/kT]}}{8\exp[E_a/kT]}\right] \qquad (7)$$

Similarly, for donor doping only, and assuming the hole density has negligible impact:

$$U_{DC} = \frac{E_g}{2} + \frac{kT}{2}\ln(N_C/N_V) - kT\ln\left[\frac{-1+\sqrt{1+8\,(N_D/N_C)\exp[E_d/kT]}}{4\exp[E_d/kT]}\right] \qquad (8)$$

Inclusion of both free carrier types was found to cause at most a five percent change from the values determined using these simple formulas. The values of N_C and N_V used are 2.9×10^{19} cm^{-3} and 1.1×10^{19} cm^{-3}, respectively, and E_g is taken to be 1.12 eV at 300 K.

These expressions assume Fermi statistics, and that the silicon sample being measured is non-degenerate. The effect of band gap narrowing on work function is ignored. Impurity ionization energies E_a and E_d of 44 meV for both boron and phosphorus are assumed. Room temperature is presumed. A band picture (to estimate WFD from the SKPM probe voltage, U_{DC}, which minimizes the electrostatic force between probe tip and doped silicon surface) is also central to these expressions (see Figure 2). Note that exponential increases in dopant concentration lead to roughly linear increases in WFD and U_{DC}, so that relative accuracy should be roughly constant over a wide range of dopant concentrations.

We have taken two tracks in the attempt to quantify doping profiles from our SKPM measurements. The first predicts the lateral surface doping profile in our contact structures using a process simulator, then applies Equations (6-8) to this doping profile to extract a predicted WFD. We proceed by validating the predicted vertical doping profile through comparison against a more traditional SIMS measurement. Figure 3 made this comparison of (1D) SIMS-determined, and SUPREM-IV [39] doping profiles in the vertical Z direction. Care was taken in the SUPREM-IV simulation to reproduce the actual implant sequence, which included four, seven degree angled implants, directed in effect at each of the four contact sides. The discrepancy between the SIMS and SUPREM-IV profiles in the tail region is relatively unimportant, since lateral diffusion should depend little on such low concentrations. The discrepancy between measured and simulated doping nearest the surface, however, causes us greater concern. We are working to adjust the SUPREM-IV parameters, to match the measured profile more fully. We then use the lateral XY surface doping profile from the same simulation, taken along a section through the contact center. These doping values combine with Equations (6-8) to predict tip-to-surface WFD.

The results of this procedure are shown in Figure 7, where comparison is also made to the measured (1D) SKPM EPD. The predicted WFD changes too sharply, and has a greater spread from maximum to minimum value. From this comparison, we draw two

important conclusions. First, the magnitude of our measured signal is reduced versus the ideal, due to screening or stray capacitance effects [35]. Second, the 'softness' in the transition from the boron to the phosphorus regions indicates the non-point nature of our measurements. Both the measured signal at XY, and the actual surface work function at XY, may be derived from contributions beyond the point XY.

In order to explore this issue further, in the second track we used *ad hoc* Gaussian-based doping profiles in a FIELDAY [40] simulation of our tip-surface system, in order to predict the WFD expected from the given profile. The results are shown in Figure 8. Qualitatively, the simulated WFD has more widely-spaced contours compared to the topography, just as we observe experimentally. In fact, the use of a numerical solution to find the WFD from the doping profile succeeds in predicting the spatial extent of the profiles, where the simple application of Equations (6-8) fails (see Figure 9). Quantitatively, however, the predicted WFD and measured EPD magnitudes still differ by an apparent scaling factor (see further discussion below).

We remark once more that one of our goals is to truly measure lateral doping profiles, to improve the ability to model lateral, as well as vertical, diffusion. Given the uncertainty in the literature of lateral dopant diffusion models, we recognize a prediction of lateral doping profile will not necessarily be valid, simply because the SIMS and SUPREM-IV profiles

compare well. However, it will serve as a point of departure for the sake of qualitative comparison.

From these two attempts, it is clear that neither the simple estimate represented by the model of Equations (6-8), nor an estimate based on the numerical solution of Poisson's equation, offers the opportunity for absolute determination of the dopant concentration, through an exact equation of estimated WFD and measured EPD (U_{DC}).

However, a relative determination can be made. The results in Figure 7 show we are able to determine relative dopant concentrations with more than sufficient sensitivity. If the maximum value of the measured EPD, shown in Figure 4, corresponds to the maximum surface dopant concentration predicted by SUPREM-IV (or used in the FIELDAY simulation); and if the minimum value of the measured EPD similarly corresponds to the minimum dopant concentration prediction; then 1 mV changes in our surface electrochemical potential measurements are related to eight percent changes in dopant concentration. This sensivity is within our ten percent goal.

With respect to our LDD measurements, Figures 5 and 6 clearly show the transition between the heavily doped drain implant region and the LDD structure. The LDD doping profile penetrates beneath the polysilicon gate and sidewall oxides spacer regions, as expected from the drive-in cycles experienced after implant. In Figure 5, the dark bands

are the source-drain regions. The three dark circular structures are the result of tungsten contacts to this diffusion region. The widths of the drain-source and lighter-contrasted channel regions are 1 μm. Comparing Figures 5 and 6, we see that the AFM image of the source-drain diffusion area has the same width as the SKPM-imaged, heavily-doped portion of the region. However, we also see the encroachment of the more lightly-contrasted LDD region into the device channel in Figure 6. This observation is consistent with expectations from the processing of these devices, and highlights the new information which SKPM makes available to process and device engineers.

The measurements shown here are only a small fraction of those we have taken. Dopants implanted into arrays of contact holes and stripes, for substrates of both polarities, have been imaged successfully, with consistent interpretation.

Clearly, however, we have only achieved part of our goal. In order to determine absolute dopant concentration from our measurements, we need to make advances in a number of areas. These are discussed as follows:

5.1 Tip and Microprobe Geometry

Ideally we would use a "dual-resonance" cantilever in order to get two distinct, and very strong, resonant peaks, at ω and Ω. Such a cantilever can be constructed using two discrete widths on the lever arm leading to the probe tip. This would increase our sensitivity

particularly in SKPM mode, since the mechanical resonance at the SKPM frequency ω is not nearly as strong as at the fundamental AFM frequency Ω. Pending incorporation of such tips, we must excite our uniformly shaped cantilever at the two best frequencies available.

We have demonstrated the reproducibility of our technique through measurements on a single contact sample, using both sharp (radius = 5 nm) and dull (radius = 100 nm) tips, over a two month period, with acceptably comparable results. With both sharp and dull tips, 300 mV peak-to-peak measurement swings were obtained on the same samples discussed in this work. Reversing the polarities of the tip-sample electrical connections (that is, grounding the tip *vs.* grounding the sample) changed the signal contrast, but not the peak-to-peak swing. Using a new, sharp tip, however, requires a large value for V_{ac}. Once the tip dulls, the value of V_{ac} required drops considerably (by as much as a factor of ten).

We have also observed the effect of stray capacitance, derived from the entire cantilever area, and not simply the tip, upon the Kelvin signal. The passage of the cantilever over substrate areas far from the tip, with inhomogeneous topographic and dopant features, can produce characteristic measurement signatures. These signatures can be reproduced using simulation [35]. Further improvements in the Kelvin technique will require modifications

in the cantilever design, to eliminate these stray capacitive effects.

5.2 Effects of Surface Physics

Dopant profiling has been done on GaAs samples, using STM in ultra-high vacuum [41]. Success with GaAs would seem to encourage application of this technique to silicon. However, the needs for a high vacuum, and for a conductive substrate, compromise our goals of speed, and ease of measurement and sample preparation. Furthermore, it has been shown that high-vacuum STM of doped silicon surfaces is unable to image dopant concentration, due to the collapse of the silicon band gap at the surface of an ultra-clean, cleaved silicon sample. Attempts to resolve this situation using H_2 to passivate the surface have been unsuccessful [42].

We believe our measurements succeed, where the high-vacuum STM measurements fail, because of the presence of a passivating, high-quality surface oxide. Our sample preparation protocol (see Table I) etches away the top 5-10 nm of SiO_2, thus removing any charged surface contaminants. The remaining oxide, grown under stringent purity requirements, will have low charge densities. The presence of an oxide does imply the possible presence of charged interface states or fixed oxide charges, even under the best of growth conditions. Previous work explored the effect of surface states on the vibrating reed Kelvin probe measurement, applied to amorphous silicon thin film growth [43]. The large

density of mid-gap states in the bulk material, characteristic of amorphous silicon, makes direct comparison to our sample system unwarranted. Nonetheless, we can still estimate the effect of charged surface states (or, if our samples are protected by thin thermal or native oxides, the effect of fixed oxide charge) in the following way. Charged surface states or fixed oxide charge will shift the flatband voltage of the tip-sample capacitor, and our Kelvin measurement, by an amount:

$$\Delta V_{flatband} = \Delta U_{DC} = q\frac{N_F\, t_{ins}}{\epsilon_{ins}} \tag{9}$$

where N_F is the surface charge density in cm^{-2}, t_{ins} is the thickness of the dielectric separating the tip and sample, and ϵ_{ins} is the dielectric constant. Presuming a dielectric of silicon dioxide, 10 nm thick, the flatband shift will be 4.7 mV for $N_F = 10^{10}$, and 47 mV for $N_F = 10^{11}$. Most thermal oxides fabricated using modern technology, on light-to-moderately doped substrates, will have N_F values easily in, or even below, this range. Minimization of the change in the Kelvin signal caused by surface charge can thus be minimized by decreasing the charge density through alternative hydrogen passivation methods [44–46], decreasing the tip-to-surface distance, or increasing the dielectric constant of the region separating the tip and surface.

Our simple analysis in Equations (6-8) presumes a uniformly doped surface. Yet, the

electrostatic force acting on a microprobe tip in the vicinity of a $p-n$ junction has an inhomogeneous character which will likely alter the interpretation of results in the vicinity of such a surface junction. We have explored these effects, using analytical and numerical simulation means [35].

We have observed the spatial and temporal effects of surface charges in our SKPM measurements, as moderate changes in the value of U_{DC} which must be applied to minimize the electrostatic force, and the cantilever resonance at frequency ω. Surface charges can be fixed spatially, as in charge trapped in an oxide [34]. Or, they can accumulate over the time scale of the SKPM scan, due to local variations in the measurement environment, which can accumulate charge on the tip. These variations may be caused by humidity [47], adsorption of air-borne particles, and related causes. We believe the environmental contributions to charging can be controlled, through improving the air and humidity control in the measurement lab.

5.3 Calibration Using Known Standards

Ideally, regardless of tip geometry, surface effects, or environmental effects, a given sample's dopant concentration should be extracted from the SKPM measurement with consistent accuracy. For this goal to be achieved, calibration must be done. Calibration is not uncommon in the measurement of 2D doping profiles. 1D SIMS profiles, for instance,

have been used to calibrate 2D isocentration contours highlighted using wet etching under UV illumination and SEM imaging [48].

Knowledge of the work function of the tip is critical to extraction of the dopant concentration. Furthermore, understanding the relationship between our tip-to-surface EPD measurements, and the doping and the surface beneath the tip, must provide the foundation of a quantitative SKPM technique. Toward this end, we are using SKPM to measure surfaces of samples with known dopant concentration over a wide XY area. These measurements will provide information to establish a quantitative relationship between dopant concentration and measured EPD. They will also allow controlled studies of the effects of surface preparation, and surface atmosphere during measurement.

5.4 Lateral Extent of Electrostatic Force

Our analysis of the SKPM technique is predicated on minimizing the electrostatic force between tip and substrate. To date, our analysis has considered Z effects only. However, our primary tip does not have the atomically sharp character necessary for our Z-only analysis to be most valid. The electric field lines connecting the tip to the substrate will have a lateral XY character, which needs to be considered. This can best be done by modifying the electrostatic force to be $\mathbf{F} = \nabla E$, where $\mathbf{F}$ is now a vector force, and E is the scalar, but now XYZ dependent, electrostatic energy.

Our analysis has also presumed charge neutrality at the substrate surface, in order to determine the the Fermi level. However, in these experiments we scan across a $p-n$ junction, which by nature includes a depletion region, which is not charge neutral. Taking this into consideration will be necessary in order to determine the absolute doping concentration.

The overall result of quantitative consideration of these factors may lead to a simple scaling relation between the measured EPD, and the WFD estimated from it. Comparison between theoretical values for the WFD and our measurements of dopant profiles have shown a consistent scaling factor of 2.5 +/- 0.1 to date. That is, after first removing a constant offset, multiplying the measured SKPM signal by this scaling factor leads to very close agreement between simulated and estimated doping profiles. An example is shown in Figure 9, where the measured SKPM signal U_{DC} has been scaled by 2.46. The scaled EPD is compared to the WFD predicted for the given structure by FIELDAY. The lateral dimensions for the measured signal are tied to the surface force gradient changes attendant to the topographic changes of the contact edge, which are also matched to the FIELDAY result. This scaling factor is unrelated to the electronics in the SKPM feedback.

6 Conclusions

We have demonstrated the application of the SKPM technique to the problem of deter-

mining dopant concentration profiles in two dimensions, at size scales below 100 nm. The technique is presently sensitive to changes in dopant concentration, from $\approx 10^{15}$ cm^{-3} to 10^{20} cm^{-3}, of less than ten percent at these size scales. Measurements are fast, and require little if any sample preparation. They are repeatable, and reproducible to the extent that changes in probe tip do not affect the measurements significantly. Calibration of our measurements against absolute dopant concentration standards remains to be demonstrated. The technique has been applied successfully to the imaging of relative doping profiles in micron-scale contact holes. It has also been used to explore the technologically significant surface doping profile of the LDD region of a MOSFET, where we have successfully imaged the LDD region by the direct means provided by SKPM. A simple equation between the measured electrochemical potential difference between the probe tip and sample surface, and the dopant concentration related work function difference, does not suffice to establish an absolute extraction of the doping profile. Predictions of the work function difference derived from two-dimensional process simulations yield good agreement, within a reproducible scaling factor attributable to the effects of surface physics.

7 Acknowledgments

The authors acknowledge the following sources with gratitude: P. Cadrecha and the management of IBM-Essex Junction, for equipment and personnel support; research sup-

port (for TH and AKH) through an IBM Shared University Research Grant, an Analog Devices (Inc.) Career Development Professorship, and Thayer School funds; C. Levey for fabrication of the SiO_2 calibration samples; M. O'Boyle of IBM-Yorktown Heights for assistance in adding the Kelvin measurement capabilities to our scanning force microscope; and D. Antoniadis of the Microsystems Technology Laboratory at MIT for support provided during a sabbatical leave (by AKH) involving this work.

References

[1] C. Hill, in *Proc. Euro. Sol. St. Dev. Res. Conf.* (Adam Hilger, Bristol, UK, 1990), pp. 53–60.

[2] R. Subrahmanyan, J. Vac. Sci. Tech. **B10**, 358 (1992).

[3] J. A. Slinkman, C. C. Williams, D. W. Abraham, and H. K. Wickramasinghe, in *IEDM Proceedings* (IEEE Press, Piscataway, NJ, 1990), pp. 73–76.

[4] C. C. Williams, J. Slinkman, W. P. Hough, and H. K. Wickramasinghe, Appl. Phys. Lett. **55**, 1662 (1989).

[5] S. H. Goodwin-Johansson, M. Ray, Y. Kim, and H. Z. Massoud, J. Vac. Sci. Tech. **B10**, 369 (1992).

[6] S. H. Goodwin-Johansson, R. Subrahmanyan, C. E. Floyd, and H. Z. Massoud, IEEE Trans. Comp.-Aided Des. **TCAD-8**, 323 (1989).

[7] M. G. Dowsett and G. A. Cooke, J. Vac. Sci. Tech. **B10**, 353 (1992).

[8] T. Takigami and M. Tanimoto, Appl. Phys. Lett. **58**, 2288 (1991).

[9] R. Subrahmanyan, H. Z. Massoud, and R. B. Fair, J. Electrochem. Soc. **137**, 1573 (1990).

[10] V. Raineri, V. Privitera, W. Vandervorst, L. Hellemans, and J. Snauwaert, Appl. Phys. Lett. **64**, 354 (1994).

[11] N. Khalil and J. Faricelli, in *Proc. Simulation of Semic. Devices and Processes (SISDEP)* (Springer-Verlag, Berlin, 1993), p. 365.

[12] C. F. Machala, J. H. Chern, J. L. Wise, and P. Yang, Texas Instruments Tech. Jour. **11**, 22 (1994).

[13] Y. Martin, D. W. Abraham, and H. K. Wickramasinghe, Appl. Phys. Lett. **52**, 1103 (1988).

[14] D. W. Abraham, C. Williams, J. Slinkman, and H. K. Wickramasinghe, J. Vac. Sci. Technol. B **9**, 703 (1991).

[15] J. M. R. Weaver and D. W. Abraham, J. Vac. Sci. Technol. B **9**, 1559 (1991).

[16] J. M. R. Weaver and H. K. Wickramasinghe, J. Vac. Sci. Technol. B **9**, 1562 (1991).

[17] M. Nonnenmacher, M. O'Boyle, and H. K. Wickramasinghe, Ultramicroscopy **42–44**, 268 (1992).

[18] L. Kelvin, Phil. Mag. **46**, 82 (1898).

[19] Y. Martin, C. C. Williams, and H. K. Wickramasinghe, J. Appl. Phys. **61**, 4723 (1987).

[20] M. Nonnenmacher, M. P. O'Boyle, and H. K. Wickramasinghe, Appl. Phys. Lett. **58**, 2921 (1991).

[21] Wye Creek Instruments, 10809 Gambrill Park Road Frederick, MD 21701.

[22] Data Translation, 100 Locke Drive Marlboro, MA 01752.

[23] EG&G Princeton Applied Research, 375 Phillips Blvd. Trenton, NJ 08618.

[24] O. Wolter, T. Bayer, and J. Greschner, J. Vac. Sci. Tech. **B9**, 1353 (1991).

[25] G. M. McClelland, R. Erlandsson, and S. Chiang, in *Review of Progress in Quantitative Nondestructive Evaluation*, edited by D. O. Thompson and D. E. Chimenti (Plenum, New York, 1987), Vol. 6B, p. 1307.

[26] H. W. Hao, A. M. Baró, and J. J. Sáenz, J. Vac. Sci. Technol. B **9**, 1323 (1991).

[27] W. A. Zisman, Rev. Sci. Instrum. **3**, 367 (1932).

[28] P. P. Craig and V. Radeka, Rev. Sci. Instrum. **41**, 258 (1970).

[29] R. Mäckel, H. Baumgärtner, and J. Ren, Rev. Sci. Instrum. **64**, 694 (1993).

[30] B. Ritty, F. Wachtel, R. Manquenouille, F. Ott, and J. B. Donnet, J. of Phys. E **15**, 310 (1982).

[31] L. B. Harris and J. Fiasson, J. of Phys. E **17**, 788 (1984).

[32] F. Rossi, Rev. Sci. Instrum. **63**, 4174 (1992).

[33] C. Schönenberger and S. F. Alvarado, Phys. Rev. Lett. **65**, 3162 (1990).

[34] T. Hochwitz, A. K. Henning, C. G. Levey, C. Daghlian, and J. Slinkman, in *Proc. 1994 IBM Failure Analysis Worldwide Technical Exchange* (IBM, Burlington, VT, Session O-5).

[35] T. Hochwitz, A. K. Henning, C. Daghlian, C. Levey, and J. Slinkman (unpublished).

[36] H. Baumgärtner, Meas. Sci. Technol. **3**, 237 (1992).

[37] Gaertner Scientific Corp., 1201 Wrightwood Chicago, IL 60614.

[38] S. Ogura, P. J. Tsang, W. W. Walker, D. L. Critchlow, and J. F. Shepard, IEEE Trans. Elec. Dev. **ED-27**, 1359 (1980).

[39] M. E. Law, C. S. Rafferty, and R. W. Dutton, SUPREM-IV User's Manual, Stanford (U.) Electronics Lab Technical Report (1989).

[40] K. A. Salsburg, P. E. Cottrell, and E. M. Buturla, in *Proc. NATO Adv. Study Inst., Process and Device Sim. for MOS-VLSI Circuits* (Martinus Nijhoff, The Hague, Netherlands, 1983), pp. 582–619.

[41] M. B. Johnson, O. Albrektsen, R. M. Feenstra, and H. W. M. Salemink, Appl. Phys. Lett. **63**, 2923 (1993).

[42] C. K. Shih, private communication (unpublished).

[43] J. K. Arch and S. J. Fonash, J. Appl. Phys. **68**, 591 (1990).

[44] L. Tsau, D. Wang, and K. L. Wang, Appl. Phys. Lett. **64**, 2113 (1994).

[45] K. Usuda, H. Kanaya, K. Yamada, T. Sato, T. Sueyoshi, and M. Iwatsuki, Appl. Phys. Lett. **64**, 3240 (1994).

[46] E. S. Snow and P. M. Campbell, Appl. Phys. Lett. **64**, 1932 (1994).

[47] T. Thundat, R. J. Warmack, G. Y. Chen, and D. P. Allison, Appl. Phys. Lett. **64**, 2894 (1994).

[48] L. Gong, A. Barthel, J. Lorenz, and H. Ryssel, in *Proc. Euro. Sol. St. Dev. Res. Conf.* (Springer-Verlag, Berlin, 1989), pp. 198–201.

8 Tables

Table I: Experimental process flow used in contact structure fabrication and simulation.

Step	Process Information
Start	Phosphorus-doped (100) silicon, 20-40 Ω-cm, 125 mm diameter
Clean	Standard RCA-type clean
Oxidation	22 nm MOS gate-quality thermal oxide
Photolithography	Mask contact holes
Ion Implantation	Boron, 10^{15} cm^{-2}, 25keV
Oxide etch	Etch oxide in contact holes
Strip Photoresist	Plasma O_2
Anneal	O_2, 5-10-5 min., dry-wet-dry, 900 C
Oxide etch	Wet oxide etch, 100:1 DI:HF, 1 min.

9 Figure Captions

Figure 1: Schematic of the scanning probe measurement system. Separate lock-in feedback loops allow simultaneous measurement of surface force gradient (AFM), and tip-to-surface electrochemical potential difference (SKPM). A laser heterodyne interferometer is used to monitor the position of the microscope tip above the sample surface.

Figure 2: Schematic of Z-direction energy bands for the tip-surface system. a) $U_{DC} = 0$: The electrostatic force between tip and surface is equal to the work function difference; b) U_{DC} has been adjusted to null the electrostatic force, and is equal to the work function difference.

Figure 3: Comparison of (1D) SIMS-determined and SUPREM-IV dopant density profiles in the vertical Z direction.

Figure 4: Contours of SKPM measurements of 2D, lateral XY tip-to-surface electrochemical potential difference.

Figure 5: AFM surface image of source-drain and channels regions in an N-channel MOSFET.

Figure 6: SKPM image of source-drain and channels regions in an N-channel MOSFET. Note the clear delineation of the change from the heavily-doped to the lightly-doped region.

Figure 7: Comparison of measured SKPM (1D) tip-to-surface electrochemical potential difference, taken along a section through the contact center, with predicted (1D) U_{DC} derived from Equation 6.

Figure 8: Two-dimensional contours of predicted tip-to-surface work function difference, based on FIELDAY simulation using Gaussian-derived dopant profiles.

Figure 9: One-dimensional SKPM scan through contact center, before and after scaling of measured potential, compared with predicted (1D) tip-to-surface work function difference derived from the FIELDAY simulation shown in Figure 8.

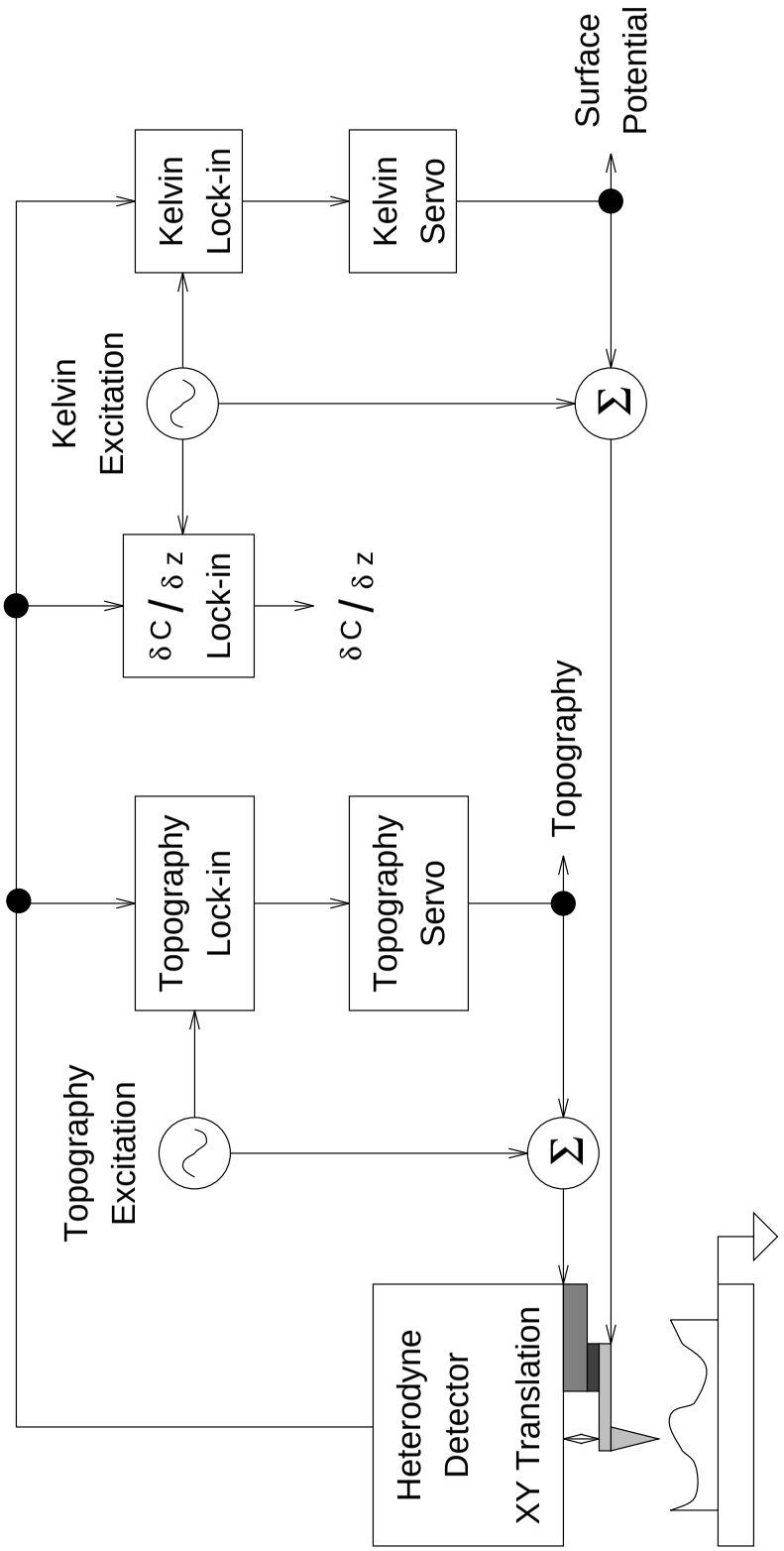

Figure 1: Henning, *et al.*, Journal of Applied Physics

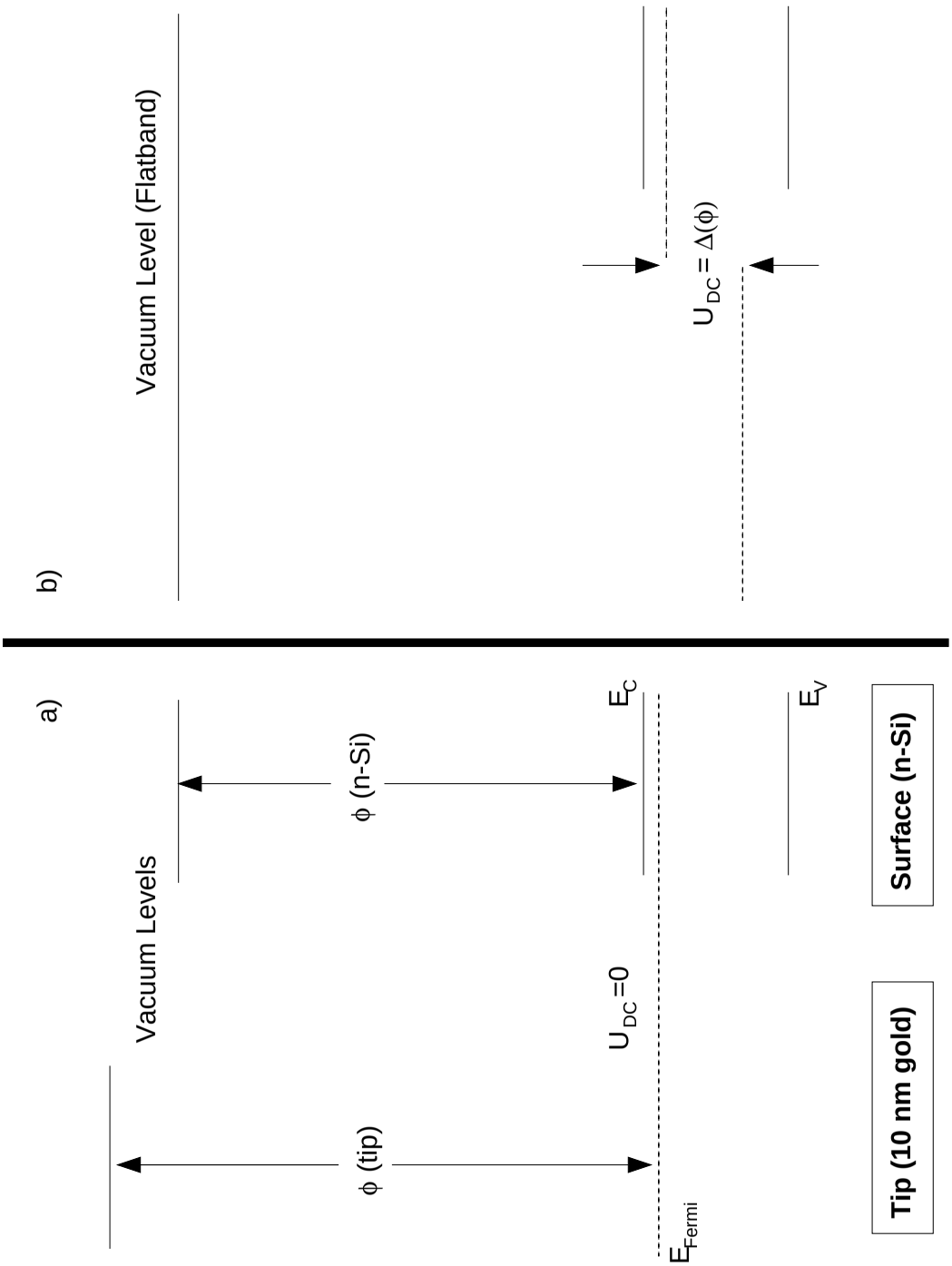

Figure 2: Henning, *et al.*, Journal of Applied Physics

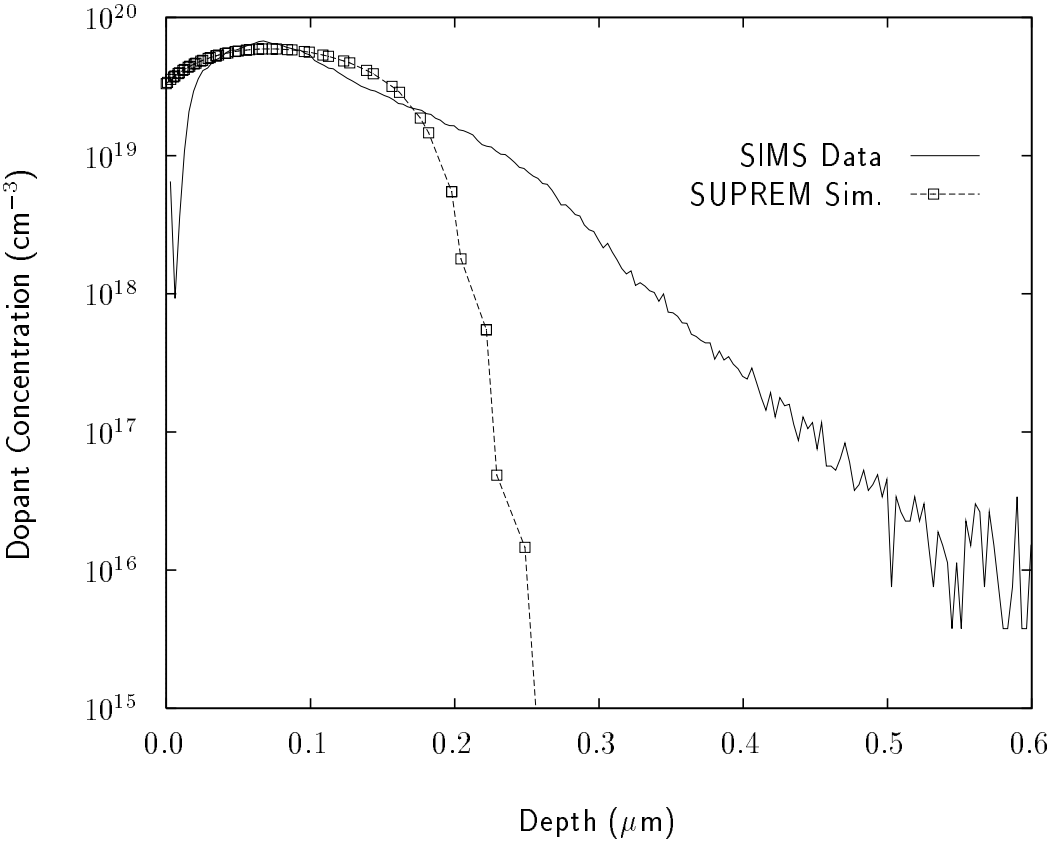

Figure 3: Henning, *et al.*, Journal of Applied Physics

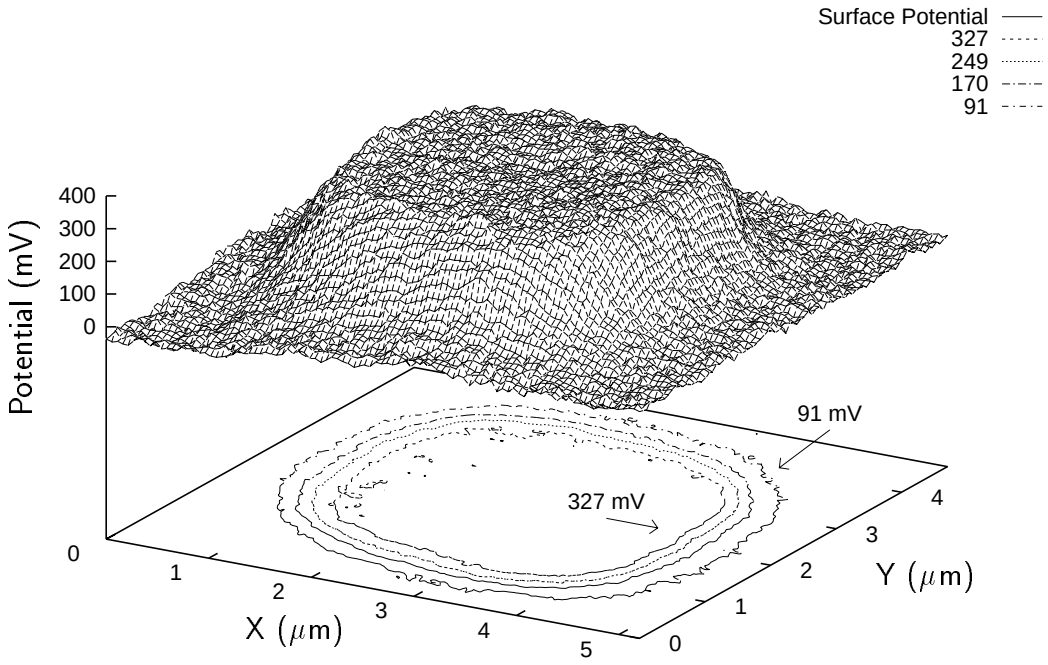

Figure 4: Henning, *et al.*, Journal of Applied Physics

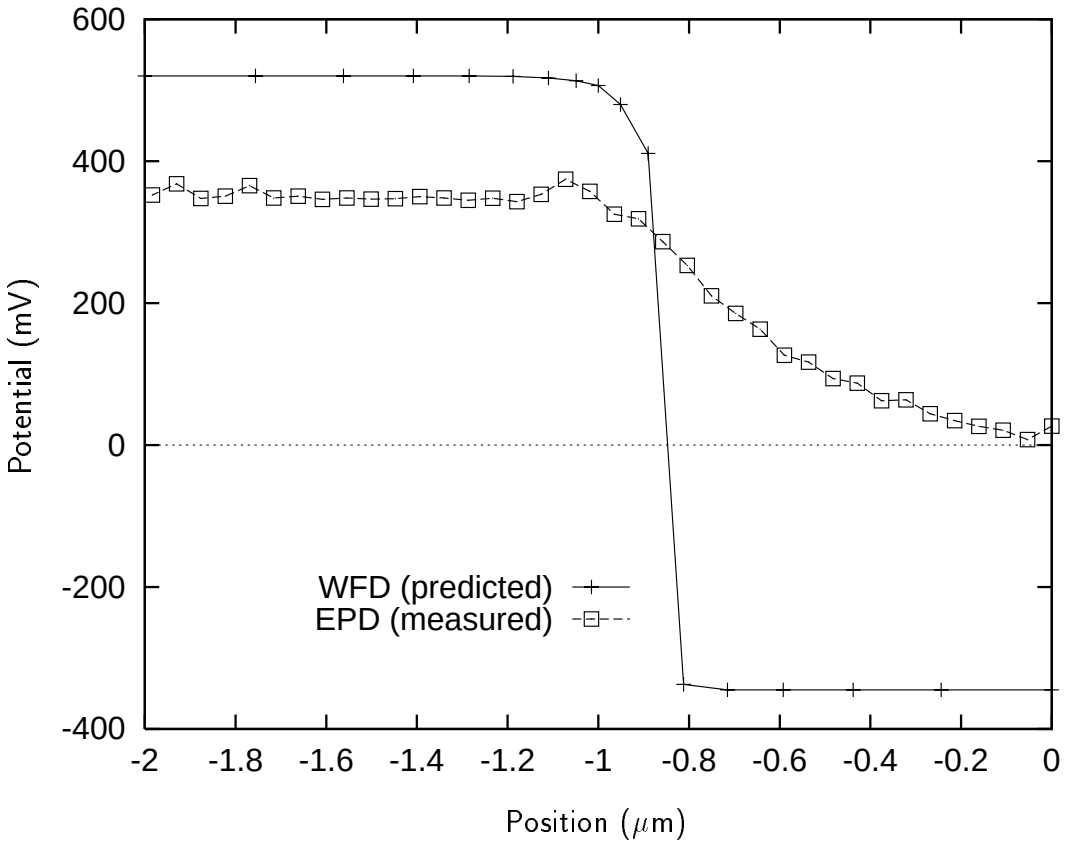

Figure 7: Henning, *et al.*, Journal of Applied Physics

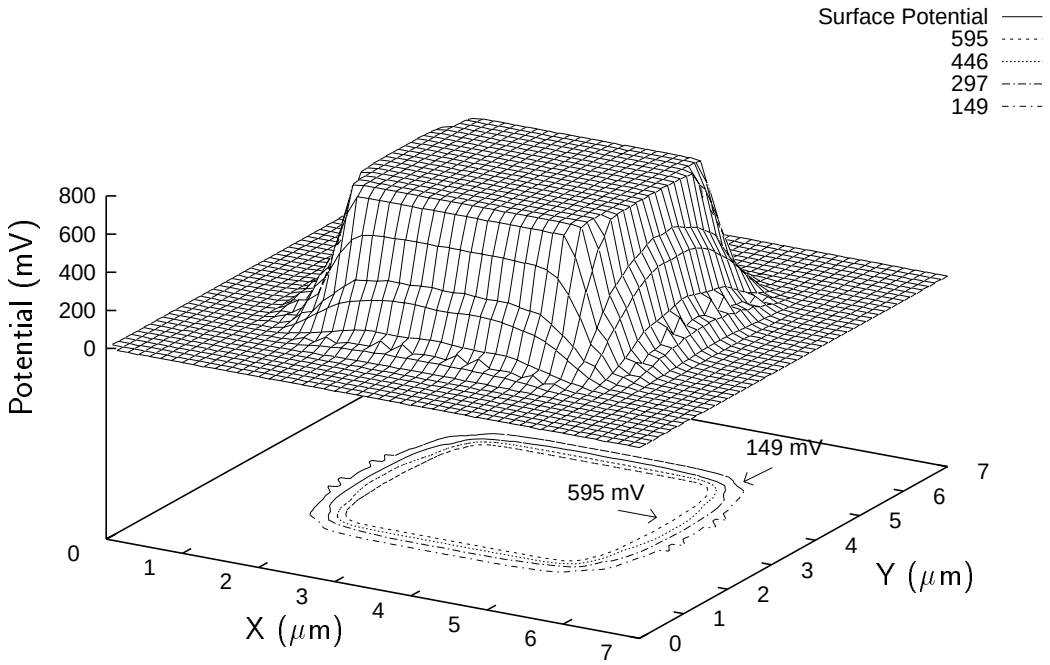

Figure 8: Henning, *et al.*, Journal of Applied Physics

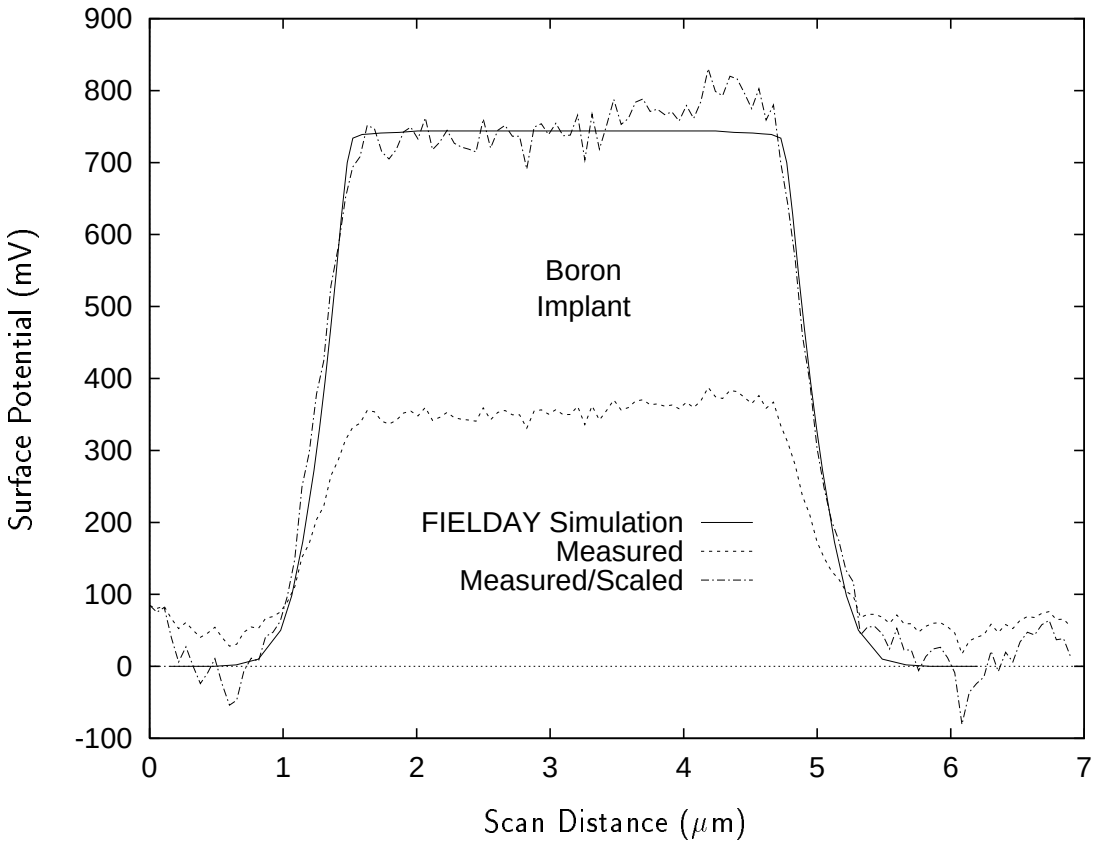

Figure 9: Henning, *et al.*, Journal of Applied Physics